Boosting the photocatalytic ability of Cu2O nanowires for CO2 conversion by MXene quantum dots

Zeng, Zhiping; Yan, Yibo; Chen, Jie; Zan, Ping; Tian, Qinghua; Chen, Peng

Boosting the Photocatalytic Ability of Cu$_2$O Nanowires for CO$_2$ Conversion by MXene Quantum Dots

Zhiping Zeng, Yibo Yan, Jie Chen, Ping Zan, Qinghua Tian and Peng Chen*

Dr. Z. Zeng, Dr. Y. Yan, J. Chen, P. Zan, Prof. P. Chen

School of Chemical and Biomedical Engineering, Nanyang Technological University, 70 Nanyang Drive, Singapore 637457, Singapore

*E-mail: chenpeng@ntu.edu.sg

Prof. Q. Tian

Department of Chemistry, School of Sciences, Zhejiang Sci-Tech University, 928 Second Avenue, Xiasha Higher Education Zone, Hangzhou 310018, PR China

Abstract

MXene quantum dots (QDs) are emerging 0D nanomaterials. Here, we develop a new heterostructure based on a 1D photoactive semiconductor and a 0D MXene QD for improved photocatalytic reduction of CO$_2$ into methanol. Specifically, Ti$_3$C$_2$ QDs are incorporated onto Cu$_2$O nanowires (NWs) through a simple self-assembly strategy. We demonstrate that Ti$_3$C$_2$ QDs not only significantly improve the stability of Cu$_2$O NWs but also greatly improve their photocatatlytic performance by enhancing charge transfer, charge transport, carrier density, light adsorption, as well as by decreasing band bending edge and charge recombination. The energy level diagram derived from both experimental measurements and theoretical calculations provide further insights of such hierarchical photocatalysis system.

1. Introduction

The excessive emission and accumulation of CO$_2$ are the serious threat to sustainable development of

earth. Therefore, tremendous efforts have been stimulated for conversion of CO_2 into clean and renewable fuels. Since the pioneer work by Halmann in 1978,[1] numerous semiconductor catalysts have been developed for photocataytic and photoelectrochemical reduction of CO_2.[2-9] Among them, p-type Cu_2O nanostructures, which desirably have a conduction band more negative than the redox potential of CO_2 and a not-too-wide bandgap (~2.2 eV) to ensure broad light absorption, have been widely explored for photo-induced conversion of CO_2.[10-14] Nevertheless, the major shortcoming of Cu_2O-based nanomaterials is the fact that Cu_2O is easily oxidized or reduced by the photo-induced charge carriers. Various strategies have thus been developed to protect active surface of Cu_2O by integration with, for examples, carbon nanomaterials,[15,16] noble metals,[17-19] or other semiconductors.[13,20-22] These methods, however, require complicated or expensive fabrication processes (e.g., atomic layer deposition, e-beam evaporation) and / or noble metals, and often give limited success.

MXenes, referring to a new class of two-dimensional (2D) transition metal carbides, nitrides, or carbonitrides, have recently attracted much attention, because MXenes offer a unique combination of good electronic conductivity, good chemical stability, and abundant active catalytic sites.[23-30] Recently, a few studies have shown the potential of MXenes in photocatalysis applications.[31-34] For instances, Ti_3C_2 sheet has been employed as an efficient co-catalyst on CdS, ZnS, TiO_2, C_3N_4 or Bi_2WO_6 to enhance their photocatalytic activities.[35-39]

0D quantum dots (QDs) derived from 2D materials (e.g., graphene quantum dots, boron nitride nanodots, and molybdenum disulfide nanodots) exhibit distinct properties as compared to their 2D counterparts, such as, bandgap widening due to quantum confinement, better tunability in physicochemical properties, more abundant active edge sites, and better dispersibility. A few recent studies have demonstrated the use of MXene QDs for cell imaging,[40] photothermal therapy,[41] pH

sensor,[42] H_2O_2 detection,[43] and sodium-ion battery.[44] Herein, we have elaborately designed hierarchical Ti_3C_2 QDs/Cu_2O nanowires (NWs)/Cu heterostructures via a progressive electrostatic self-assembly strategy for solar-driven CO_2 conversion. We demonstrate that T_3C_2 QDs greatly enhance the photocatalytic activity and the stability of Cu_2O NWs. The synergistic cooperation of 0D T_3C_2 QDs and 1D Cu_2O NWs is disclosed and the photo-induced conversion mechanism is further revealed based on density functional theory (DFT) calculation.

2. Results and discussion
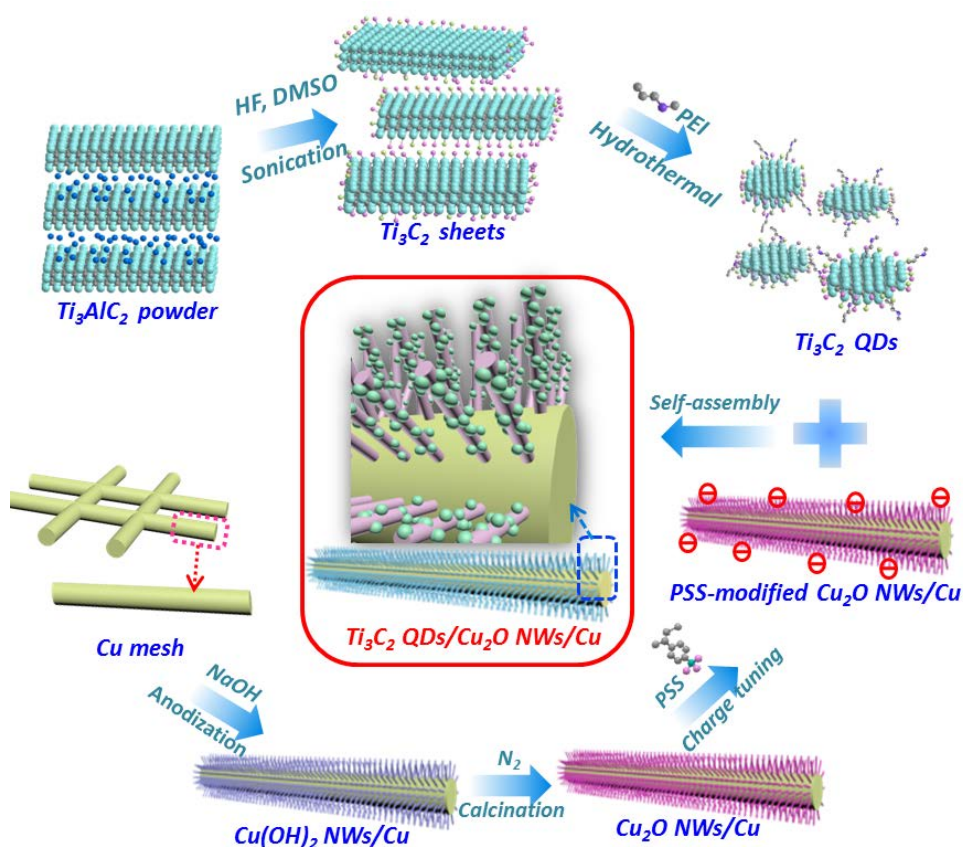
Figure 1. Schematic illustration for preparing Ti_3C_2 QDs and Ti_3C_2 QDs/Cu_2O NWs/Cu heterostructure.

As illustrated in **Figure 1**, Ti_3AlC_2 powder firstly reacts with hydrofluoric acid to etch away aluminum layers,[27] resulting accordion-like Ti_3C_2 structures (**Figure S1**, Supporting Information). The Ti_3C_2 layers are terminated with surface moieties (a mixture of -OH, =O, and -F) to replace aluminum.

Subjecting to strong ultrasonication in a protective atmosphere, the layered Ti_3C_2 structures are broken into Ti_3C_2 microsheets (**Figure S2,** Supporting Information). Finally, functionalized Ti_3C_2 quantum dots (QDs) were obtained by hydrothermally cutting Ti_3C_2 sheets and passivated by polyethylenimine (PEI) (**Figure S3,** Supporting Information). The size, morphologies, surface charge, composition and elemental analysis of Ti_3C_2 QDs and Ti_3C_2 sheets are presented in **Figure S2-S6** (Supporting Information).
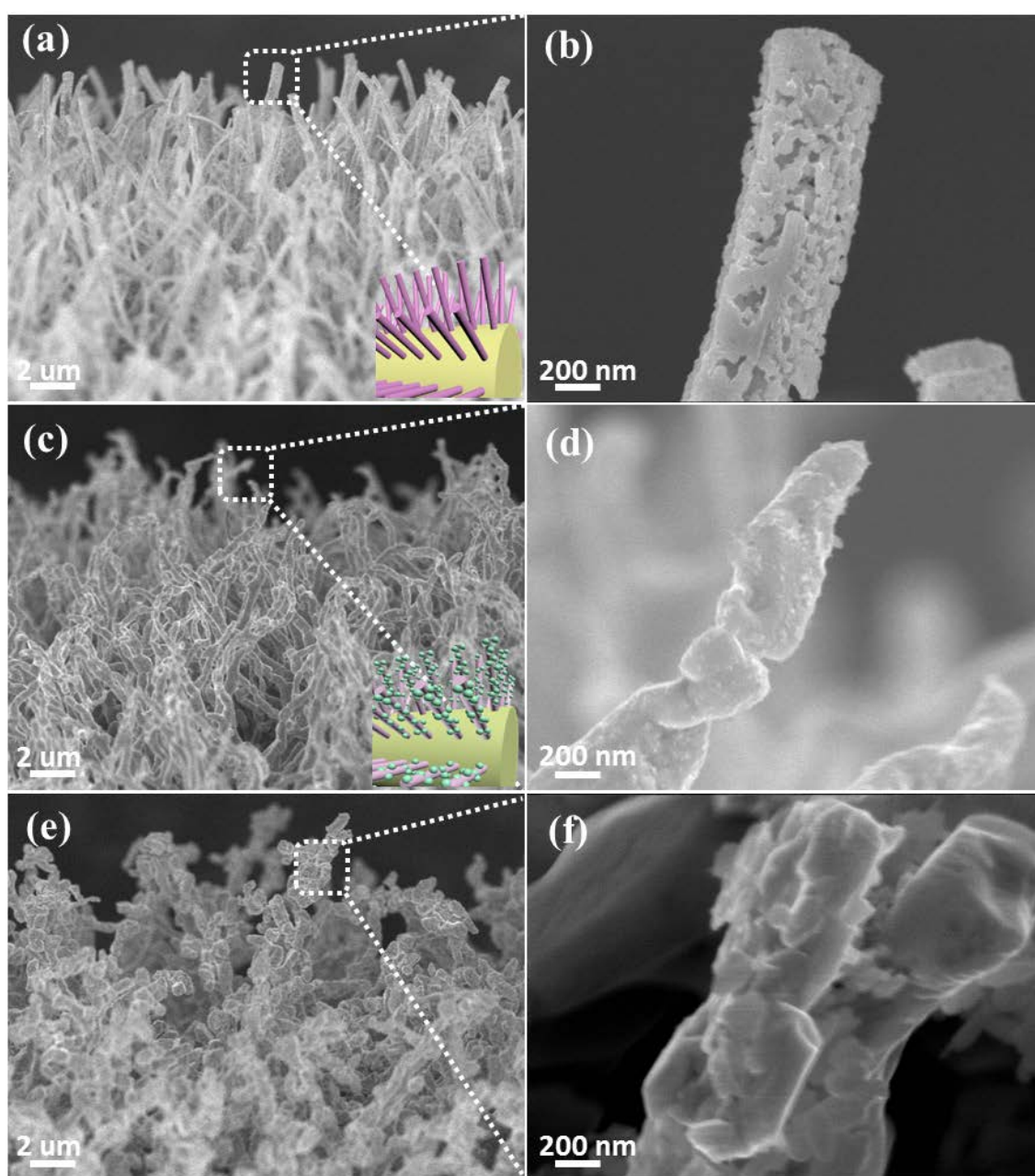
Figure 2. FESEM images of (a, b) Cu_2O NWs/Cu, (c, d) Ti_3C_2 QDs/Cu_2O NWs/Cu, and (e, f) Ti_3C_2 sheets/Cu_2O NWs/Cu heterostructures.

As compared with other nanostructures, semiconductor nanowires have both long optical paths for efficient light absorption and short charge transport distances, whereby ensuring collection of the photogenerated charge carriers before they combine.[45] Cu_2O NWs are desirable for light harvesting.[46] As shown in **Figure 1**, $Cu(OH)_2$ NWs/Cu mesh is first obtained by anodizing Cu mesh in an alkali solution and red Cu_2O NWs/Cu mesh is then produced after calcination in N_2 atmosphere at 550 °C. As revealed by electron scanning microscopy (SEM), Cu_2O NWs have a porous surface and a diameter of ~500 nm (**Figure 2a,b**). After being treated with poly(sodium 4-styrenesulfonate) (PSS) to afford a negatively charged surface on Cu_2O NWs, Ti_3C_2 QDs grafted with positively charged PEI are electrostatically self-assembled onto Cu_2O NWs forming hierarchical Ti_3C_2 QDs/Cu_2O NWs/Cu heterostructure. PSS and PEI molecules are completely eliminated by the subsequent calcination process in argon atmosphere, leaving Ti_3C_2 QDs and Cu_2O NWs in intimate contact. Coating by Ti_3C_2 QD doesn't obviously alter the overall morphology of Cu_2O NWs but covers their porous surfaces (**Figure 2c,d**). Successful deposition of Ti_3C_2 QDs is also confirmed by elemental mapping (**Figure S8,** Supporting Information). As shown by transmission electron microscopy (TEM) and high-resolution TEM (HRTEM), abundant Ti_3C_2 QDs are uniformly immobilized on Cu_2O NWs with intimate contact (**Figure 3a,b**). This is also evidenced by the uniform distribution of Ti, C, Cu, O elements uncovered by elemental mapping (**Figure 3c-g**). N element is absent although the synthesis is under N_2 atmosphere. For comparison, Ti_3C_2 sheets/Cu_2O NWs/Cu heterostructure has also been similarly fabricated and deposition of Ti_3C_2 sheets (~200×300 nm, **Figure S2,** Supporting Information) on Cu_2O NWs is evidenced by SEM (**Figure 2e,f**) and TEM (**Figure 3h,i**).

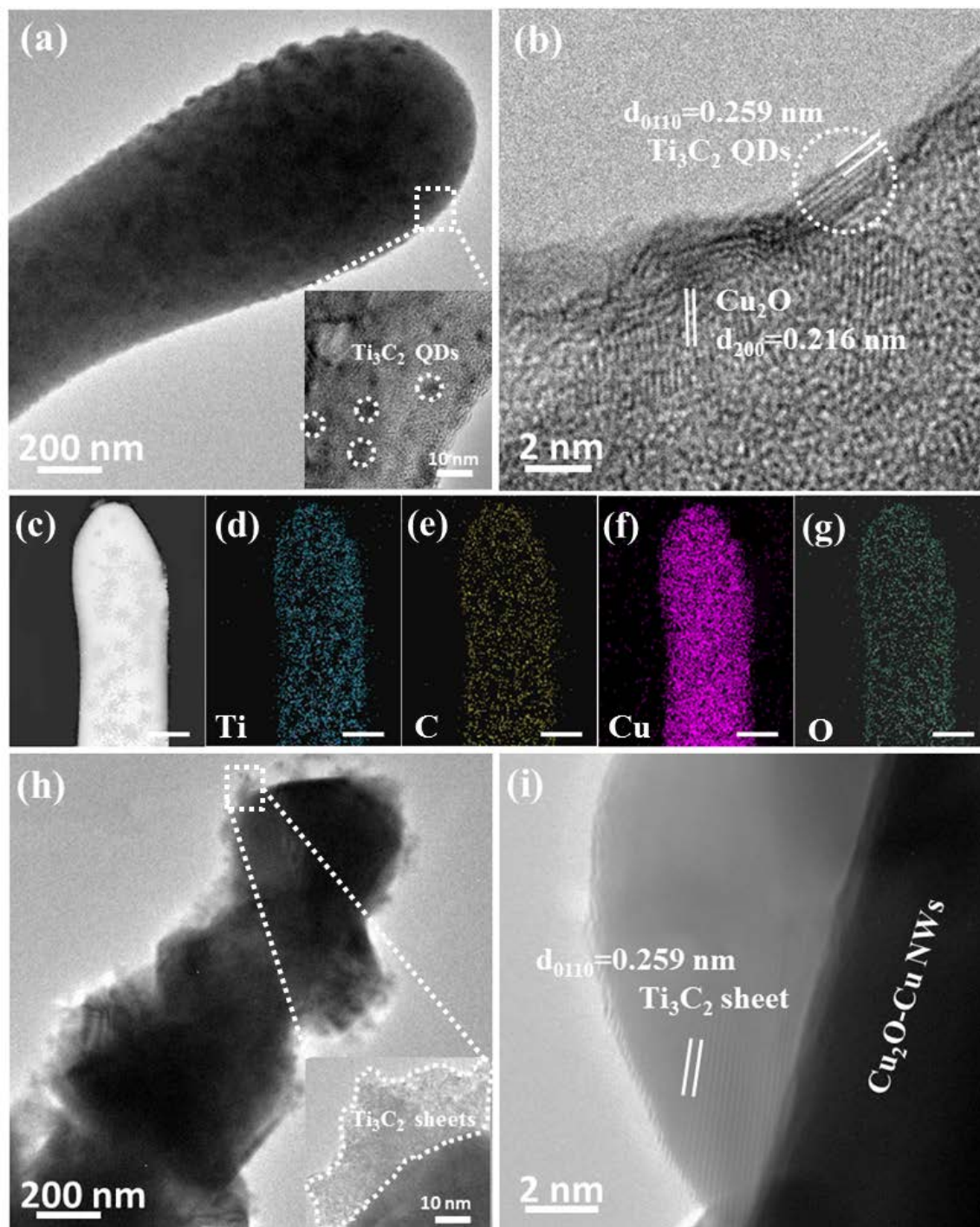**Figure 3**. (a) TEM image of Ti_3C_2 QDs/Cu_2O NWs/Cu heterostructure with a magnified region shown in inset. (b) HRTEM image of Ti_3C_2 QDs/Cu_2O NWs/Cu. (c) Dark field-STEM image of Ti_3C_2 QDs/Cu_2O NWs/Cu. (d-g) EDX elemental mapping spectra. Scale bar = 200 nm. (h) TEM image of Ti_3C_2 sheets/Cu_2O NWs/Cu with a magnified region shown in inset. (i) HRTEM image of Ti_3C_2 sheets/Cu_2O NWs/Cu.
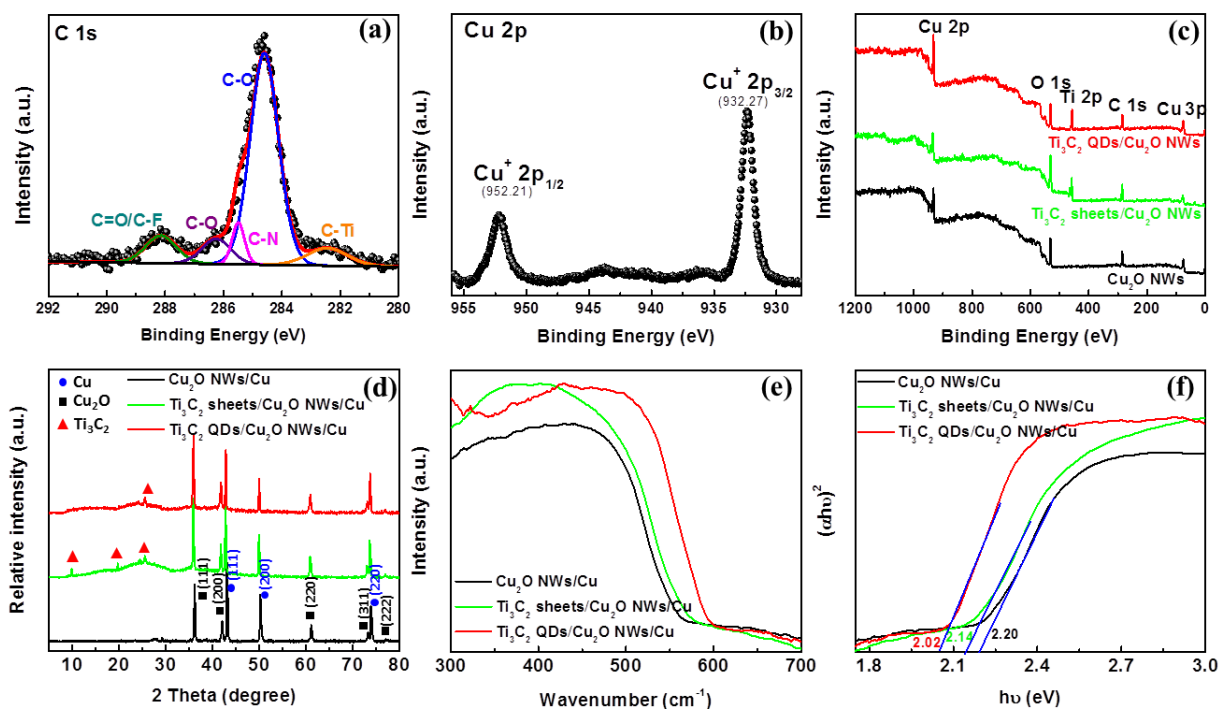
Figure 4. (a, b) High-resolution XPS spectra of C 1s and Cu 2p of Ti$_3$C$_2$ QDs/Cu$_2$O NWs/Cu. (c) XPS survey spectra, (d) XRD patterns, (e) UV-vis diffuse reflectance spectra (DRS), and (f) the plots of transformed Kubelka-Munk function of Cu$_2$O NWs/Cu, Ti$_3$C$_2$ sheets/Cu$_2$O NWs/Cu, and Ti$_3$C$_2$ QDs/Cu$_2$O NWs/Cu heterostructures.

Successful fabrication of Cu$_2$O NWs/Cu mesh, Ti$_3$C$_2$ sheets/Cu$_2$O NWs/Cu and Ti$_3$C$_2$ QDs/Cu$_2$O NWs/Cu heterostructures is also corroborated by the appearance of Cu 2p, Ti 2p, and C 1s peaks in the high-resolution X-ray photoelectron spectroscopy (XPS) spectra (**Figure 4a,b,** and **Figure S9,S10,** Supporting Information). Deposition of Ti$_3$C$_2$ samples on Cu$_2$O NWs/Cu is further confirmed by FTIR spectra where the peaks at 1629.2 cm^{-1}, 1028.6 cm^{-1}, and 561.4 cm^{-1} correspond to the stretching vibration modes of C=O, C-F and Ti-O groups grafted onto Ti$_3$C$_2$ during synthesis (**Figure S11a,** Supporting Information). Moreover, self-assembly of Ti$_3$C$_2$ samples on Cu$_2$O NWs/Cu is evidenced by Raman signals at 1383 cm^{-1} and 1612 cm^{-1} which are in accordance with the D and G bands of Ti$_3$C$_2$ samples (**Figure S5b, S11b,** Supporting Information). As shown by X-ray diffraction (XRD) (**Figure 4d**), all the samples show diffraction peaks at 36.2°, 42.1°, 61.2°, 73.2°, and 77.3°, which are assigned to the (111), (200), (220), (311), and (222) planes of Cu$_2$O (JCPDS No. 75-1531).[47] Heterostructures

7

with Ti3C2 QDs or Ti3C2 sheets present an amorphous carbon signal at around 24°.[40]

UV-vis diffuse reflectance spectroscopy (DRS) shows that decoration of Ti_3C_2 sheets on Cu_2O NWs/Cu enhances the light absorption efficiency while decoration of Ti_3C_2 QDs enhances both efficiency and range of light adsorption (**Figure 4e**). Strong light adsorption is desirable for photocatalysis. The bandgap can be estimated from the plot of $(\alpha\text{-}h\upsilon)^2$ versus photon energy, as shown in **Figure 4f**. The bandgap, obtained by extrapolating the maximum slope, is 2.02 eV for Ti_3C_2 QDs/Cu_2O NWs/Cu, which is smaller than that of Cu_2O (2.2 eV) and Ti_3C_2 sheets/Cu_2O NWs/Cu (2.14 eV), suggesting the better light absorption ability of Ti_3C_2 QDs/Cu_2O NWs/Cu.
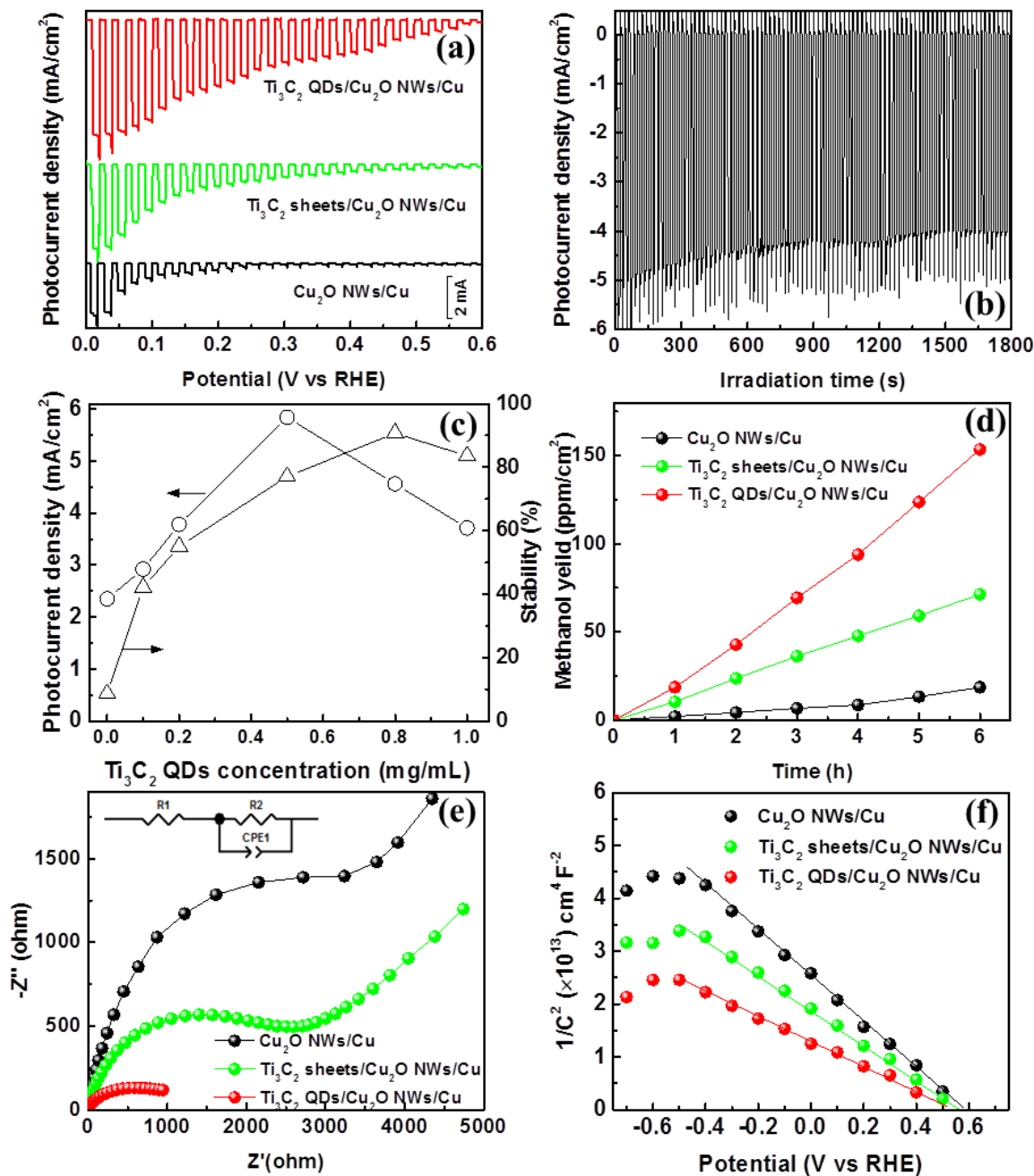
Figure 5. (a) Photoelectrochemical performance of Cu_2O NWs/Cu, Ti_3C_2 sheets/Cu_2O NWs/Cu, and Ti_3C_2 QDs/Cu_2O NWs/Cu. (b) Photoelectrochemical stability measurement of Ti_3C_2 QDs/Cu_2O NWs/Cu. (c) Photocurrent densities (at 0 V vs RHE; left axis) and photostability (right axis) of Ti_3C_2 QDs/Cu_2O NWs/Cu using different concentrations of Ti_3C_2 QDs. (d) Yields of methanol as a function of time. (e) Nyquist plots from electrochemical impedance spectroscopy (EIS). (f) Mott-Schottky plots.

As shown in **Figure 5a**, the photocurrent of Ti_3C_2 QDs/Cu_2O NWs/Cu is the greatest among the

three heterostructures, attributable to improved light absorption, charge separation and transport

facilitated by Ti_3C_2 QDs. The photostability of Ti_3C_2 QDs/Cu_2O NWs/Cu is also the best as compared

9

the other heterostructures (**Figure 5a**, **S12,** and **S13** in Supporting Information). The poor stability of bare Cu_2O NWs due to easy oxidation greatly limits their use. Our experiments confirm the protective roles of Ti_3C_2 and suggest that Cu_2O NWs have better contact with Ti_3C_2 QDs than Ti_3C_2 sheets. As demonstrated in **Figure 5c** and **Figure S14** (Supporting Information), initial increase of Ti_3C_2 QD concentration improves the photocurrent, but a too high concentration does the opposite because Ti_3C_2 QDs block too much light adsorption of Cu_2O NWs. Photostability is also enhanced by increasing Ti_3C_2 QD concentration until reach a plateau. In the following experiments, the optimal concentration of Ti_3C_2 QDs (0.5 mg/mL) was used.

The performance of all three Cu_2O-based photocatalysts for CO_2 photoreduction was evaluated over 6 hours. ^{1}H NMR and gas chromatography (GC) (**Figure S15, S16** and **S17** in Supporting Information) show that CH_3OH is essentially the only product from CO_2 photoreduction. Ti_3C_2 QDs/Cu_2O NWs/Cu gives the highest methanol yield of 153.38 ppm cm^{-2}, which is 8.25 times of that from Cu_2O NWs/Cu and 2.15 times of that from Ti_3C_2 sheets/Cu_2O NWs/Cu. For Ti_3C_2 QDs/Cu_2O NWs/Cu, a production rate of 25.77 ppm cm^{-2} h^{-1} is achieved, outperforming other Cu_2O-based and Ti_3C_2-based catalysts (see comparison in **Table S1,** Supporting Information). This production rate is equivalent to 78.50 µmol g^{-1} h^{-1}, which is an over-underestimation of the catalyst capability because the weight of Cu mesh is included in the calculation. As shown in **Figure S16b** (Supporting Information), after 6 cycles, the rate of methanol yield remains as 89% of that from the first run, indicating the stable photocatalytic activity of Ti_3C_2 QDs/Cu_2O NWs/Cu. In addition, a control experiment was conducted to show that PSS-modification doesn't enhance Cu_2O NW's photocatalytic performance (**Table S1** in Supporting Information). Finally, using isotopically labeled [13]CO_2 as the carbon source, we verify that produced methanol is solely from CO_2 reduction (**Figure S18** in Supporting Information).

To understand the mechanisms underlying the performance enhancement by the synergistic integration between Ti_3C_2 QDs and Cu_2O NWs, electrochemical impedance spectroscopy (EIS) was performed. As shown in **Figure 5e**, the charge transfer resistance of Ti_3C_2 QDs/Cu_2O NWs/Cu, as indicated by the radius of the preceding semi-circle in the EIS spectrum, is the smallest as compared to that of Ti_3C_2 sheets/Cu_2O NWs/Cu and Cu_2O NWs/Cu, suggesting that Ti_3C_2 QDs can largely enhance the charge transfer. Mott-Schottky (M-S) plots obtained from photoelectrochemical measurement under illumination by the simulated solar light are shown in **Figure 5f.** The negative slope of the relationship between $1/C^2$ (where C is capacitance) and applied potential indicates the p-type semiconductance of Cu_2O. The flat band potentials of Cu_2O NWs/Cu, Ti_3C_2 sheets/Cu_2O NWs/Cu and Ti_3C_2 QDs/Cu_2O NWs/Cu, determined by the linear extrapolation of $1/C^2$, are 0.59 V, 0.56 V and 0.52 V (*vs.* RHE), respectively. This observation suggests that Ti_3C_2 QDs cause an apparent decrease in band bending edge at the junction with Cu_2O NWs. Further, the carrier density N_D can be determined from the linear region of M-S plots based on the following equation:[48] $N_D = - (2 / e\varepsilon\varepsilon_0)[dU/d(1/C^2)]$, where $e = 1.6 \times 10^{-19}$ C, $\varepsilon = 7.5$ for Cu_2O,[49] $\varepsilon_0 = 8.86 \times 10^{-12}$ F m^{-1}, and U is applied potential. The N_D of Cu_2O NWs/Cu, Ti_3C_2 sheets/Cu_2O NWs/Cu, and Ti_3C_2 QDs/Cu_2O NWs/Cu heterostructures is calculated to be 1.09×10^{19}, 1.89×10^{19}, 2.75×10^{19} cm^{-3}, respectively. This implies that Ti_3C_2 QDs can largely increase the carrier density, presumably attributable to their ability to improve light adsorption (see also **Figure 4e**) and charge separation. Taken together, the enhanced CO_2 reduction performance of Ti_3C_2 QDs/Cu_2O NWs/Cu is owing to the abilities of Ti_3C_2 QDs to promote charge transfer, decrease band bending edge, and increase carrier density.
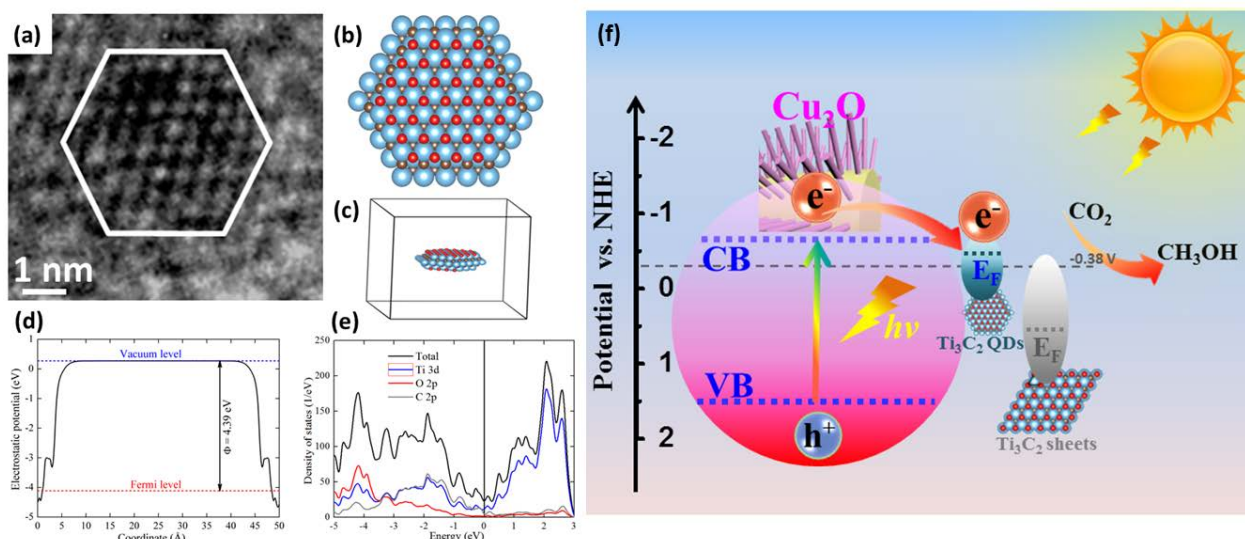
Figure 6. (a) High-resolution TEM image of a Ti_3C_2 QD. (b-e) the top view, side view of structure, calculated Femi level, and DOS of O-terminated Ti_3C_2 QD model. (f) Energy level diagram of Ti_3C_2 QDs/Cu_2O NWs/Cu and Ti_3C_2 sheets/Cu_2O NWs/Cu heterostructures.

Based on the high-resolution TEM image of a Ti_3C_2 QD (**Figure 6a**), the optimized (strain-free) structure is depicted in **Figure 6b,c**. The Fermi level (E_F *vs.* vacuum level) and electronic structure of O-terminated Ti_3C_2 QDs are determined by density functional theory (DFT) calculation (**Figure 6d**). Density of states (DOS) of Ti_3C_2 QDs exhibits numerous electronic states cross the Fermi level (**Figure 6e**), suggesting the excellent conductivity of Ti_3C_2 QDs, which is beneficial for electron transport. Energy level structure diagram of the heterostructure systems is illustrated in **Figure 6f**. The valence band (VB) and conductive band (CB) of Cu_2O NWs are determined to be 1.497 V and -0.703 V (*vs. NHE*, pH=7). E_F (*vs. NHE*, pH=7) of Ti_3C_2 QDs is calculated to be -0.523 V according to **Figure 6d** while E_F of the Ti_3C_2 sheets is reported to be 0.71 V (*vs. NHE*, pH=7).[37]

Under simulated solar light irradiation, electrons are photo-excited from the VB of Cu_2O to its CB. As Ti_3C_2 QD is highly conductive and its E_F is less negative than the CB of Cu_2O, the photo-excited electrons tend to transfer to the QD and accumulate instead of being recombined within Cu_2O. And because the E_F of Ti_3C_2 QD is more negative than the redox potential of CO_2 to methanol, the

accumulated electrons stimulate this reduction reaction. Moreover, Ti_3C_2 prefers to chemisorb CO_2 instead of H_2O, and further facilitates CO_2 reduction by promoting H^+ attachment and readily donating electrons.[50,51] Although MXene may be oxidized or hydroxylated during the reaction, these oxygenated groups on Ti_3C_2 can actually further enhance CO_2 adsorption and interaction with the intermediate carbonated products.[52] We propose that the CO_2 reduction to methanol is a six-electron-transfer process as shown in **Figure S19** (Supporting Information). The reduction of CO_2 to CO cannot easily occur because the standard redox potential for this reaction (-0.53 V *vs* NHE) is more negative than the Fermi level of Ti_3C_2 QDs. In comparison, the E_F of Ti_3C_2 sheets is positive which is not desirable for catalyzing the reaction. This diagram explains why Ti_3C_2 QDs/Cu_2O NWs outperforms Ti_3C_2 sheets/Cu_2O NWs and Cu_2O NWs.

3. Conclusion

In summary, a hierarchical heterostructure, specifically Ti_3C_2 QDs decorated Cu_2O NWs on Cu mesh, has been constructed via simple electrostatic self-assembly. Methanol production resulting from the photocatalytic reduction of CO_2 by Ti_3C_2 QDs/Cu_2O NWs/Cu is 8.25 times or 2.15 times of that from Cu_2O NWs/Cu or Ti_3C_2 sheets/Cu_2O NWs/Cu, respectively. We demonstrate both experimentally and theoretically that Ti_3C_2 QDs not only significantly improve the stability of Cu_2O NWs but also greatly improve their photocatalytic performance by enhancing charge transfer, charge transport, carrier density, light adsorption, as well as by decreasing band bending edge and charge recombination. MXene QDs are new 0D nanomaterials which have recently attracted considerable research interest because of their unique properties. This study adds a new dimension to their application scope.

4. Experimental section

Synthesis of Cu$_2$O/Cu mesh photocathode: The Cu mesh (Alfa Aesar, wire diameter of 0.11 mm) was anodized in 3.0 M NaOH solution for 30 min at a current density of 10 mA/cm^2 to produce Cu(OH)$_2$ NWs/Cu mesh. The Cu(OH)$_2$ NWs/Cu mesh was calcinated at 550 °C at N$_2$ atmosphere for 4 h to obtain Cu$_2$O NWs/Cu mesh.

Preparation of Ti$_3$C$_2$ sheets and Ti$_3$C$_2$ quantum dots: 2.0 g Ti$_3$AlC$_2$ power (Nanjing Mission Materials Co. Ltd.) was immersed in 20 mL of 48 wt% hydrofluoric acid (HF, VWR chemicals) with stirring for 18 h to obtain a stable suspension. The suspension was centrifuged to obtain the solid Ti$_3$C$_2$ powder, which was then washed multiple times with deionized (DI) water and dried under vacuum at 60 °C for 12 h. 1.0 g of Ti$_3$C$_2$ was mixed with 20 mL of dimethyl sulfoxide (DMSO) for 20 h, followed by centrifugation at 3500 rpm for 5 min. The precipitate was dispersed in DI water at a mass ratio of 1:300, with argon gas being continuously bubbled and sonication for 3h. The prepared solution was centrifuged at 3500 rpm for 20 min to remove unexfoliated particles, leaving suspended Ti$_3$C$_2$ sheets. Subsequently, polyethylenimine (PEI) was added to the dispersion and heated at 120 °C in N$_2$ atmosphere for 5 h. The solution was dialyzed with a dialysis bag (MWCD: 10k Da) for 3 days, producing the positively-charged PEI-modified Ti$_3$C$_2$ sheets. The Ti$_3$C$_2$ sheets was finally concentrated by a rotatory evaporator and freeze-dried for further usage.

The dispersion of Ti$_3$C$_2$ sheets (without PEI modification) was tip-sonicated under argon atmosphere for 6 h at 120 W. Then, the dispersion was bath sonicated continuously for 10 h at a power of 300 W. Then PEI was added to the dispersion and heated at 120 °C at N$_2$ atmosphere for overnight. The suspension was filtered using 220 nm membrane. The positively-charged Ti$_3$C$_2$ quantum dots (QDs) are obtained by dialyzing the filtered solution with a dialysis bag (MWCD: 1000 Da) for three days. Ti$_3$C$_2$ QDs was finally concentrated by a rotatory evaporator and freeze-dried for further usage.

Preparation of Ti$_3$C$_2$ QDs/Cu$_2$O NWs/Cu and Ti$_3$C$_2$ sheets/Cu$_2$O NWs/Cu heterostructures: Cu$_2$O NWs/Cu mesh was dipped into poly(sodium 4-styrenesulfonate) (PSS) solution (1% volume in ethanol) for 2 h at 90 ℃, thoroughly washed with ethanol for three times and dried with a gentle N$_2$ stream. PSS-modified Cu$_2$O NWs/Cu was immersed into positively-charged PEI-modified Ti$_3$C$_2$ QDs solutions with different concentrations for 24 h under ambient condition, then washed with DI water, and dried with a N$_2$ stream. Finally, self-assembled Ti$_3$C$_2$ QDs/Cu$_2$O NWs/Cu heterostructure electrodes were calcined in argon atmosphere at 200 °C for 1 h. Ti$_3$C$_2$ sheets/Cu$_2$O NWs/Cu heterostructure electrode was fabricated similarly, except using Ti$_3$C$_2$ sheet solution instead.

Characterization: Scanning electron microscopy (SEM) and energy dispersive spectroscopy (EDS) images were acquired with field emission scanning electron microscopy (JEOL, JSM-6700F). Transmission electron

microscopy (TEM) images were obtained by using a JEOL JEM 2010F. Scanning transmission electron microscopy (STEM)-energy dispersive X-ray (EDX) elemental mapping images were collected by a JEOL JEM 2100F instrument. UV-vis diffuse reflectance spectra (DRS) were obtained by a UV-vis-NIR spectrometer (Varian Cary 500 Scan) with $BaSO_4$ as the background. X-ray photoelectron spectroscopy (XPS) spectra were collected on a photoelectron spectrometer (ESCALAB 250, Thermo Fisher Scientific), and binding energy (BE) of the element was calibrated based on the BE of carbon (284.60 eV). Crystal structure was explored by X-ray diffraction (Brucker D8, 40 kV, 40 mA) using Cu Kα as the radiation source. Fourier transform infrared (FTIR) spectra were recorded on a PerkinElmer FTIR spectrometer. Photoluminescence (PL) spectra were collected by an LP920-KS instrument. Atomic force microscopy (AFM, MFP3D, Asylum Research) images were taken using the tapping mode. Dynamic light scattering analysis (Zeta PALS, Brookhaven Instruments Co.) was used to determine the Zeta potential. Raman spectra were collected on a RenishawinVia Raman System 1000. Photoreduction product of isotopically labeled $^{13}CO_2$ was determined by GC-MS (Agilent, GC 6890N, MS 5973). ^{1}H nuclear magnetic resonance (^{1}H NMR, Avance 300 NMR) was employed to analyze the product, for which dimethylsulfoxide (DMSO) was used as the internal standard.

Photoelectrochemical (PEC) measurements: PEC measurements were carried out by an electrochemical workstation (Zennium, Zahner), using the standard three-electrode configuration (platinum plate as the counter and Ag/AgCl as the reference) and a medium containing 20 mL Na_2SO_4 (0.5 M, pH=5.8 with potassium phosphate 0.1 M). Our heterostructure electrodes (20 mm × 10 mm) were vertically dipped into electrolyte and irradiated with a 300 W Xenon arc lamp (Newport) equipped with an AM 1.5 filter.

Photochemical reduction of carbon dioxide: The photocatalytic reactions were carried out in a 100 mL quartz bottle with a screw cap. Before the experiment, high purity CO_2 gas was bubbled into 80 mL H_2O for 1 h to reach the saturation solubility. Cu_2O-based heterostructures (2 cm^2) were vertically hung in the cell and irradiated by a 300 W Xe lamp. The gas chromatograph (GC) was employed to analyze the products, using follows inlet temperature of 250 ºC, Mol Sieve columns, 30 m of capillary column, and temperature-rise from 80 ºC, then 10 ºC/min to 150 ºC, holding 2 min, and then cooling.

Density functional theory (DFT) calculation: First-principles calculations were performed using the QUANTUM-ESPRESSO Package.[53] Spin-polarized Perdew-Burke-Ernzerhof exchange correlation function was used to describe the exchange-correlation.[54,55] A cutoff energy of 60 Ry was used for the plane-wave expansion.[56] For simulating Ti_3C_2 QD, we used a hexagonal cluster with a diameter of 24.3 Å, comprising 303 atoms (133 Ti, 96 C and 74 O atoms). The model was calculated by placing it inside a 50 Å × 50 Å × 50 Å space,

leading to vacuum layers of at least 25 Å. The Brillouin zone was sampled by a $1 \times 1 \times 1$ k-mesh. The geometry was optimized until all residual forces were below 0.02 eV/Å. According to the obtained work function (-4.39 eV $vs.$ Vacuum level) of O-terminated Ti_3C_2 QDs and the conversion formula of E_F ($vs.$ NHE) and E_F ($vs.$ Vacuum level), E_F($vs.$ NHE, pH=0) = -4.5 V - E_F ($vs.$ Vacuum level), and the Nernst equation E($vs.$ NHE, pH=7) = E($vs.$ NHE, pH=0) - 0.059pH, E_F ($vs.$ NHE, pH=7) of O-terminated Ti_3C_2 QDs can be calculated to be -0.523 V.

$Conductive\ band\ and\ valence\ band\ of\ Cu_2O$: According to the Mulliken electronegativity theory, the position of valence band (VB) and conduction band (CB) of Cu_2O can be calculated via the following equations:[57,58] E_{VB} = χ - E_e + 0.5 E_g, E_{CB} = E_{VB} - E_g, where χ is the Mulliken electro-negativity of the semiconductor (5.32 eV for Cu_2O[59]), E_e is the energy of free electrons versus hydrogen (4.5 eV), E_g is the bandgap energy of the semiconductor. According to the bandgap of Cu_2O obtained by UV-Vis DRS measurement, E_{CB} and E_{VB} of Cu_2O are calculated to be -0.703 V and 1.497 V (vs. NHE, pH=7), respectively.

Supporting Information

Supporting Information is available from the Wiley Online Library.

Acknowledgement

Conflict of Interest

The authors declare no competing financial interest.

Keywords

MXene quantum dots, Cu_2O nanowires, CO_2 reduction, photocatalysis

Reference

[1] M. Halmann, *Nature* **1978**, *275*, 115.
[2] S. Chu, Y. Cui, N. Liu, *Nat. Mater.* **2017**, *16*, 16.
[3] M. Mikkelsen, M. Jorgensen, F. C. Krebs, *Energy Environ. Sci.* **2010**, *3*, 43.
[4] S. N. Habisreutinger, L. Schmidt-Mende, J. K. Stolarczyk, *Angew Chem. Int. Ed.* **2013**, *52*, 7372.
[5] X. Zheng, L. Zhang, *Energy Environ. Sci.* **2016**, *9*, 2511.
[6] M. Xiao, Z. Wang, M. Lyu, B. Luo, S. Wang, G. Liu, H.-M. Cheng, L. Wang, *Adv. Mater.* **2018**, 1801369.
[7] J. Ran, M. Jaroniec, S. Z. Qiao, *Adv. Mater.* **2018**, 30, 1704649; g) Y. Yan, J. Chen, N. Li, J. Tian, K. Li, J. Jiang, J. Liu, Q. Tian, P. Chen, *ACS Nano* **2018**, *12*, 3523.

[8]   Z. Sun, J. M. T. A. Fischer, Q. A. Li, J. Hu, Q. Tang, H. Wang, Z. Wu, M. Hankel, D. J. Searles, L. Wang, *Appl. Catal. B Environ.* **2017**, *216*, 146.

[9]   W. -J. Ong, L. K. Putri, Y. -C. Tan, L. -L. Tan, N. Li, Y. H. Ng, X. Wen, S. -P. Chai, *Nano Res.* **2017**, *10*, 1673.

[10] H. Li, X. Zhang, D. R. MacFarlane, *Adv. Energy Mater.* **2015**, *5*, 1401077.

[11] C. W. Li, M. W. Kanan, *J. Am. Chem. Soc.* **2012**, *134*, 7231.

[12] F. Li, L. Zhang, J. Tong, Y. Liu, S. Xu, Y. Cao, S. Cao, *Nano Energy* **2016**, *27*, 320.

[13] M. Schreier, J. Luo, P. Gao, T. Moehl, M. T. Mayer, M. Gratzel, *J. Am. Chem. Soc.* **2016**, *138*, 1938.

[14] G. Ghadimkhani, N. R. Tacconi, W. Chanmanee, C. Janaky, K. Rajeshwar, *Chem. Commun.* **2013**, *49*, 1297.

[15] Z. Zhang, R. Dua, L. Zhang, H. Zhu, H. Zhang, P. Wang, *ACS Nano* **2013**, *7*, 1709.

[16] E. Kecsenovity, B. Endrodi, P. S. Toth, Y. Zou, R. A. W. Dryfe, K. Rajeshwar, C. Janaky, *J. Am. Chem. Soc.* **2017**, *139*, 6682.

[17] M. A. Mahmoud, W. Qian, M. A. El-Sayed, *Nano Lett.* **2011**, *11*, 3285.

[18] K. H. Yang, S. C. Hsu, M. H. Huang, *Chem. Mater.* **2016**, *28*, 5140.

[19] J. W. Hong, D. H. Wi, S. U. Lee, S. W. Han, *J. Am. Chem. Soc.* **2016**, *138*, 15766.

[20] A. Paracchino, V. Laporte, K. Sivula, M. Gratzel, E. Thimsen, *Nat. Mater.* **2011**, *10*, 456.

[21] C. G. Morales-Guio, S. D. Tilley, H. Vrubel, M. Gratzel, X. Hu, *Nat. Commun.* **2014**, *5*, 3059

[22] J. S. Luo, L. Steier, M. K. Son, M. Schreier, M. T. Mayer, M. Gratzel, *Nano Lett.* **2016**, *16*, 1848.

[23] O. Mashtalir, M. R. Lukatskaya, M. Q. Zhao, M. W. Barsoum, Y. Gogotsi, *Adv. Mater.* **2015**, *27*, 3501.

[24] Y. Y. Peng, B. Akuzum, N. Kurra, M. Q. Zhao, M. Alhabe, B. Anasori, E. C. Kumbur, H. N. Alshareef, M. D. Ger, Y. Gogotsi, *Energy Environ. Sci.* **2016**, *9*, 2847.

[25] Q. Tao, M. Dahlqvist, J. Lu, S. Kota, R. Meshkian, J. Halim, J. Palisaitis, L. Hultman, M. W. Barsoum, P. O. A. Persson, J. Rosen, *Nat. Commun.* **2017**, *8*, 14949.

[26] M. Ghidiu, M. R. Lukatskaya, M. Q. Zhao, Y. Gogotsi, M. W. Barsoum, *Nature* **2014**, *516*, 78.

[27] M. Naguib, M. Kurtoglu, V. Presser, J. Lu, J. Niu, M. Heon, L. Hultman, Y. Gogotsi, M. W. Barsoum, *Adv. Mater.* **2011**, *23*, 4248.

[28] X. Wang, S. Kajiyama, H. Iinuma, E. Hosono, S. Oro, I. Moriguchi, M. Okubo, A. Yamada, *Nat. Commun.* **2015**, *6*, 6544.

[29] M. Q. Zhao, C. E. Ren, Z. Ling, M. R. Lukatskaya, C. Zhang, K. L. Van Aken, M. W. Barsoum, Y. Gogotsi, *Adv. Mater.* **2015**, 27, 339; h) T. Y. Ma, J. L. Cao, M. Jaroniec, S. Z. Qiao, *Angew. Chem. Int. Ed.* **2016**, *55*, 1138.

[30] L. M. Azofra, N. Li, D. R. Macfarlane, C. Sun, *Energy Environ. Sci.* **2016**, *9*, 2545.

[31] M. Naguib, V. N. Mochalin, M. W. Barsoum, Y. Gogotsi, *Adv. Mater.* **2014**, *26*, 992.

[32] H. Wang, Y. Wu, X. Yuan, G. Zeng, J. Zhou, X. Wang, J. W. Chew, *Adv. Mater.* **2018**, *30*, 1704561.

[33] J. Peng, X. Chen, W. -J. Ong, X. Zhao, N. Li, *Chem* 2018, DOI: 10.1016/j.chempr.2018.08.037.

[34] Q. Xu, W. Cai, W. Li, T. S. Sreeprasad, Z. He, W. -J. Ong, N. Li, *Mater. Today Energy* **2018**, *10*, 222.

[35] J. Ran, G. Gao, F. T. Li, T. Y. Ma, A. Du, S. Z. Qiao, *Nat. Commun.* **2017**, *8*, 13907.

[36] J. Low, L. Zhang, T. Tong, B. Shen, J. Yu, *J. Catal.* **2018**, *361*, 255.

[37] S. Cao, B. Shen, T. Tong, J. Fu, J. Yu, *Adv. Funct. Mater.* **2018**, *28*, 1800136.

[38] Y. Sun, D. Jin, Y. Sun, X. Meng, Y. Gao, Y. Dall'Agnese, G. Chen, X. F. Wang, *J. Mater. Chem. A* **2018**, *6*, 9124.

[39] Y. Xu, S. Wang, J. Yang, B. Han, R. Nie, J. Wang, J. Wang, H. Jing, *Nano Energy* **2018**, *51*, 442.

[40] Q. Xue, H. Zhang, M. Zhu, Z. Pei, H. Li, Z. Wang, Y. Huang, Y. Huang, Q. Deng, J. Zhou, S. Du, Q. Huang, C. Zhi, *Adv. Mater.* **2017**, *29*, 1604847.

[41] X. Yu, X. Cai, H. Cui, S. W. Lee, X. F. Yu, B. Liu, *Nanoscale* **2017**, *9*, 17859.

[42] X. Chen, X. Sun, W. Xu, G. Pan, D. Zhou, J. Zhu, H. Wang, X. Bai, B. A. Dong, H. Song, *Nanoscale* **2018**, *10*, 1111.

[43] Q. Xu, L. Ding, Y. Wen, W. Yang, H. Zhou, X. Chen, J. Street, A. Zhou, W. J. Ong, N. Li, *J. Mater. Chem. C* **2018**, *6*, 6360.

[44] T. Zhang, X. Jiang, G. Li, Q. Yao, J. Y. Lee, *ChemNanoMat* **2018**, *4*, 56.

[45] S. W. Boettcher, J. M. Spurgeon, M. C. Putnam, E. L. Warren, D. B. Turner-Evans, M. D. Kelzenberg, J. R. Maiolo, H. A. Atwater, N. S. Lewis, *Science* **2010**, *327*, 185.

[46] L. Pan, J. H. Kim, M. T. Mayer, M. K. Son, A. Ummadisingu, J. S. Lee, A. Hagfeldt, J. Luo, M. Grätzel, *Nat. Catalysis* **2018**, *1*, 412.

[47] X. Li, Y. Qian, T. Liu, F. Cao, Z. Zang, X. Sun, S. Sun, Q. Niu, J. Wu, *J. Mater. Sci.* **2018**, *53*, 11078.

[48] Z. Li, Z. Zhang, *Nano Res.* **2018**, *11*, 1530.

[49] J. W. Hodby, T. E. Jenkins, C. Schwab, H. Tamura, D. Trivich, *J. Phys. C. Solid State Phys.* **1976**, *9*, 1429.

[50] N. Li, X. Chen, W. -J. Ong, D. R. MacFarlane, X. Zhao, A. K. Cheetham, C. Sun, *ACS Nano* **2017**, *11*, 10825.

[51] A. D. Handoko, K. H. Khoo, T. L. Tan, H. Jin, Z. W. She, *J. Mater. Chem A* **2018**, DOI: 10.1039/C8TA06567E.

[52] M. Ye, X. Wang, E. Liu, J. Ye, D. Wang, *ChemSusChem* **2018**, *11*, 1.

[53] P. Giannozzi, S. Baroni, N. Bonini, M. Calandra, R. Car, C. Cavazzoni, D. Ceresoli, G. L. Chiarotti, M. Cococcioni, I. Dabo, A. Dal Corso, S. de Gironcoli, S. Fabris, G. Fratesi, R. Gebauer, U. Gerstmann, C. Gougoussis, A. Kokalj, M. Lazzeri, L. Martin-Samos, N. Marzari, F. Mauri, R. Mazzarello, S. Paolini, A. Pasquarello, L. Paulatto, C. Sbraccia, S. Scandolo, G. Sclauzero, A. P. Seitsonen, A. Smogunov, P. Umari, R. M. Wentzcovitch, *J. Phys. Condens. Matter* **2009**, *21*, 395502.

[54] J. P. Perdew, K. Burke, M. Ernzerhof, *Phys. Rev. Lett.* **1996**, *77*, 3865.

[55] M. Khazaei, A. Ranjbar, M. Arai, T. Sasaki, S. Yunoki, *J. Mater. Chem. C* 2017, *5*, 2488.

[56] H. J. Monkhorst, J. D. Pack, *Phys. Rev. B* **1976**, *13*, 5188.

[57] a) J. P. Perdew, R. G. Parr, M. Levy, J. L. Balduz, *Phys. Rev. Lett.* **1982**, *49*, 1691.

[58] M. Singh, D. Jampaiah, A. E. Kandjani, Y. M. Sabri, E. Della Gaspera, P. Reineck, M. Judd, J. Langley, N. Cox, J. van Embden, E. L. H. Mayes, B. C. Gibson, S. K. Bhargava, R. Ramanathan, V. Bansal, *Nanoscale* **2018**, *10*, 6039.

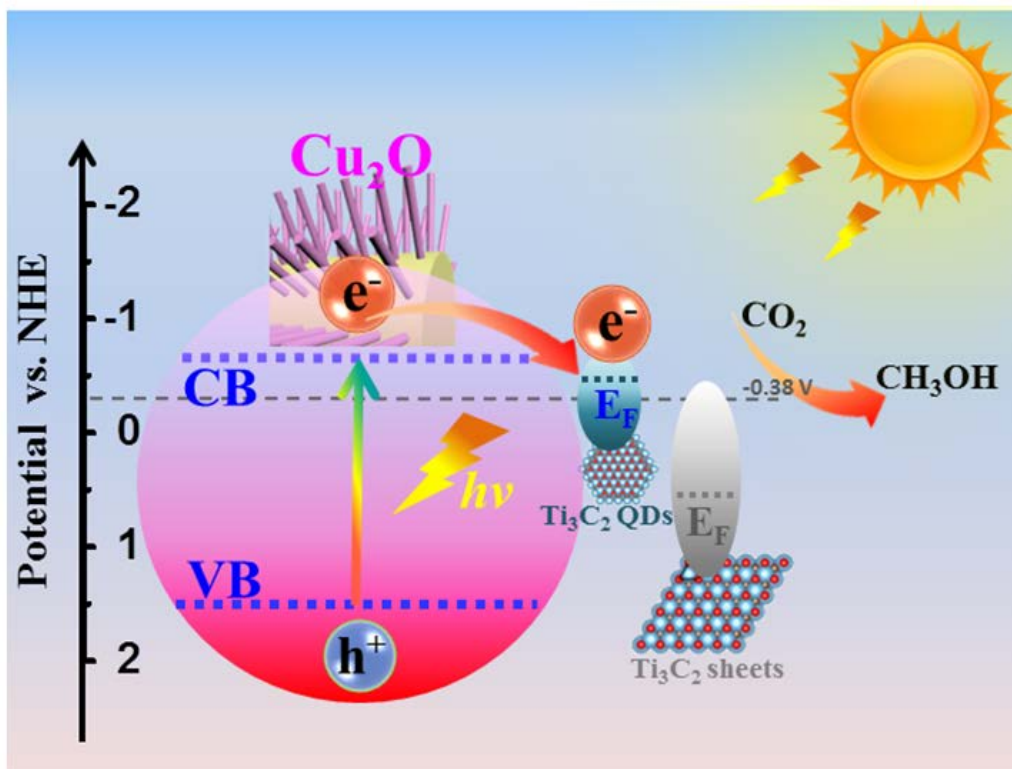[59] Y. Xu, M. A. A. Schoonen, *Am. Mineral.* **2000**, *85*, 543.

Table of contents

Ti$_3$C$_2$ quantum dots greatly enhance the photocatalytic ability of Cu$_2$O Nanowires for CO$_2$ conversion by promoting charge transfer, decreasing band bending edge, and increasing carrier density.